The Land Mobile Satellite Communication Channel—Recording, Statistics, and Channel Model

Erich Lutz, Daniel Cygan, Michael Dippold, Frank Dolainsky, and Wolfgang Papke

Abstract—**The communication channel between the MARECS satellite at 26° W and a cruising van was measured and recorded in European areas exhibiting satellite elevations from 13 to 43 deg. Different environments and mobile antennas were tested. Results of an extensive statistical evaluation include spectra of the fading amplitude, probability density, and distribution of the received signal power, as well as the percentage of time for fade and nonfade periods. Based on the physical phenomena of multipath fading and signal shadowing, an analog model of the land mobile satellite channel is developed which can readily be used for software and hardware fading simulation. The most important parameter of this model is the time-share of shadowing A, ranging from less than 1% on southern highways to 89% in the city of Stockholm. The Rice-factor c, which characterizes the channel during unshadowed periods, can vary from 3.9 to 18.1 dB. For analytical purposes the land mobile satellite channel can be represented by a digital two-state Gilbert-Elliott model. For DPSK modulation with a 10 dB signal-to-noise ratio in the satellite link, the mean bit error probability in the unshadowed channel state is typically in the range of 10^{-4}–10^{-2}, while it is around 0.3 in the shadowed channel state. With regard to data transmission, block error probability density (probability of m errors occurring in a block of n bits), error gap distribution, and block error probability are discussed. The results show good agreement between the recorded channel and the channel models. Moreover, if the transmission scheme is suitably adapted to the channel behavior, reliable and efficient data transmission via the land mobile satellite channel should be achievable.**

I. Introduction

FOR some years many activities aimed at the introduction of land mobile satellite communication services have been undertaken by different organizations all over the world. For example, MSAT-X of NASA, U.S. [1], [2]; MSAT Program of DOC, Canada [3]; experimental program of Japan [4]; Mobilesat of AUSSAT, Australia [5]; and PRODAT of ESA [6]. Finally, INMARSAT is expanding into the area of land mobile services using the operational maritime standard-C system as an initial base [7]. Field tests are also being conducted on satellite paging [8].

Satellite communications with land mobile terminals suffer from strong variations of the received signal power due to signal shadowing and multipath fading. Shadowing of the satellite signal by obstacles in the propagation path (buildings, bridges, trees, etc.) results in attenuation over the total signal bandwidth. This attenuation increases with carrier frequency, i.e., it is more marked at L-band than at UHF. For low satellite elevation the shadowed areas are larger than for high elevation. Multipath fading occurs because the satellite signal is received not only via the direct path but also after being reflected from objects in the surroundings. Due to their different propagation distances, multipath signals can add destructively resulting in a deep fade.

Therefore, for all types of land mobile systems, the communication link between the satellite and the mobile terminal is the most critical part of the transmission path and limits the performance of the total system. The introduction of a judicious fade margin into the link budget has substantial consequences for the system cost. The link availability determines the achievable throughput efficiency and the resulting message delay. Furthermore, the time-varying behavior of the land mobile satellite link must be considered when choosing a modulation scheme as well as when designing channel access and error protection methods [9]. Also, carrier recovery, bit timing, and frame synchronization have to be adapted carefully to the channel behavior. For these reasons it is essential to thoroughly investigate the characteristics of the land mobile satellite link. Propagation measurements of the L-band land mobile link have been carried out in different geographical areas and different types of environments in the U.S. and Canada [10]–[12].

From 1984 to 1987 DFVLR[1] performed several series of channel recording experiments in Europe. These tests were narrow-band measurements at a single frequency, representing the channel within its coherence bandwidth [13]. The unmodulated test carrier was transmitted from the ESA ground station in Villafranca, Spain, and relayed by the geostationary satellite MARECS at L-band (1.54 GHz). The test carrier was transmitted right-hand circularly polarized with an EIRP of 28 dBW. The receiver signal-to-noise ratio was typically 25–30 dB for a 50-Hz receiver bandwidth. The L-band carrier was received by a cruising van equipped with different antennas according to Table I. All antenna patterns were horizontally symmetrical to avoid antenna steering. The antennas with toroidal patterns exhibit vertical selectivity.

The measurements were conducted in areas with different satellite elevations; Stockholm (13°), Copenhagen (18°),

Manuscript received May 10, 1989; revised July 27, 1990 and October 16, 1990.

The authors are with the Institute for Communications Technology, German Aerospace Research Establishment, DLR, D-8031 Oberpfaffenhofen, Germany.

IEEE Log Number 9143058.

[1] At the beginning of 1989 DFVLR was renamed DLR.

0018-9545/91/0500-0375$01.00

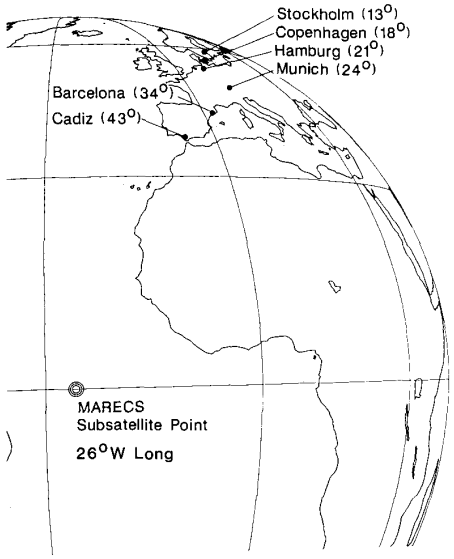

Fig. 1. Areas of land mobile channel measurements as viewed from MARECS.

TABLE I
ANTENNAS USED FOR LAND MOBILE SATELLITE CHANNEL RECORDINGS

Antenna	Antenna Type	Nominal Gain	Antenna Pattern
C3	Conical spiral	3 dBi	Hemispherical
M2	Microstrip	2 dBi	Broad toroidal
D5	Drooping crossed dipole	5 dBi	Toroidal
S6	Cylindrical slot	6 dBi	Toroidal

Hamburg (21°), Munich (24°), Barcelona (34°), and Cadiz (43°). Fig. 1 shows the measurement areas as viewed from the MARECS satellite. The test courses were carefully selected to represent different types of environments (city, suburbs, rural roads, highway) and to comprise a mixture of cruising directions. A recording experiment typically lasted from 30 to 60 min.

The received carrier was downconverted to baseband, and its inphase and quadrature components were continuously recorded on magnetic tape. The recorded time-varying behavior of the land mobile channel can be reproduced in amplitude and in phase for stored channel tests [14], and for statistical analysis.

In Section II, results of the statistical evaluation of the recordings are presented. In addition to fade depth statistics, distributions of fade durations and non-fade durations are given. In Section III, two types of models for the land mobile satellite channel are developed. The analog channel model not only yields an analytic approximation of the received signal power distribution but also models the time-dependent behavior of the complex fading process and the shadowing. A digital channel model reproduces the statistics of the bit error sequence. In Section IV, block error statistics are used to compare the behavior of the channel models and of the recorded channel.

II. Statistical Evaluation of Channel Recordings

After an initial quick-look test, the analog tape recordings were digitized and transferred to a mainframe computer for

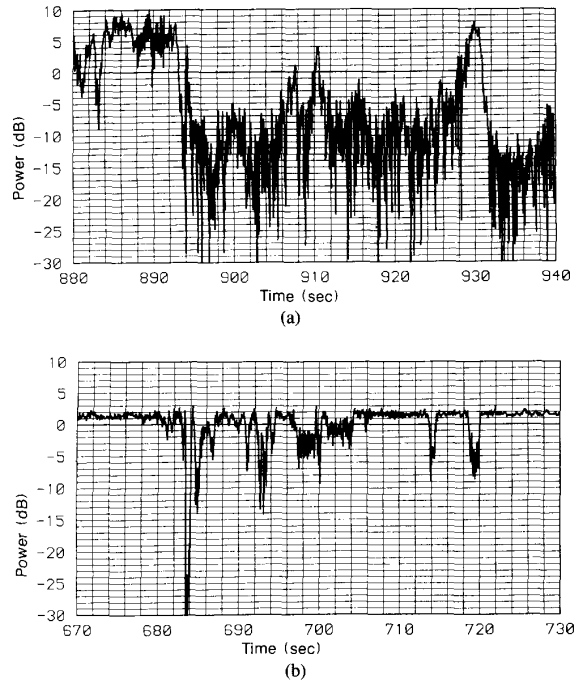

Fig. 2. Received power level. 0 dB = mean received power. (a) City, antenna S6, v = 10 km/h, 24° satellite elevation. (b) Highway, antenna S6, v = 60 km/h, 24° satellite elevation.

statistical evaluation. Fig. 2(a) shows an example of the received signal power from a channel recording in an area with narrow streets in the old city of Munich. The figure shows a high-frequency fading process which is superimposed on a low-frequency shadowing process. Relatively "good" and very "bad" channel periods can be distinguished, having a mean level difference of approximately 15 dB. For instance, a crossroad permits an unobstructed "view" of the satellite from 928 to 932 s, while before and after this period the satellite is hidden by multistory flats. Fig. 2(b) shows the received signal power from a recording on a highway. For this case and for most of the time, only small level variations due to multipath fading predominate. At 684 s, total shadowing is caused by a bridge. Further shadowing events are caused by trees, etc.

In all recordings, the vehicle velocity v was kept constant to allow easy conversion between time, velocity, or distance. The distance of the fading events is determined by the stationary electromagnetic field and is independent of the mobile velocity. Since velocity = distance/time, the time duration of the fading events is inversely proportional to the velocity of the mobile terminal.

Fig. 3(a) shows the power spectral density of the fading signal amplitude for a short measurement period in a dense city environment. The power spectral density of the amplitude fading extends to 11 Hz and does not show a clear cutoff frequency. This was probably caused by variations in mobile speed and by signal components arriving from various elevations. In open areas, the power spectral density shows no peaking but decreases with frequency as shown in Fig. 3(b).

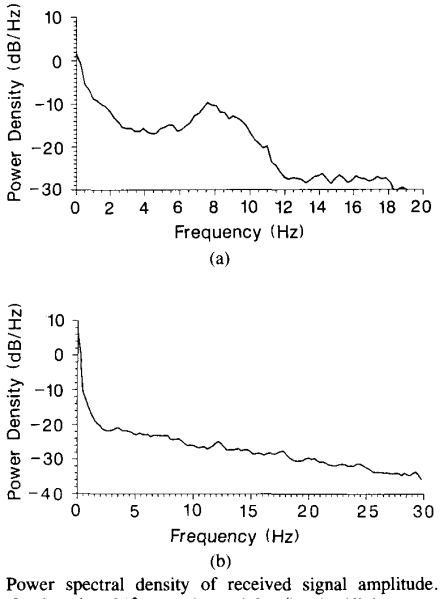

Fig. 3. Power spectral density of received signal amplitude. (a) City, antenna D5, elevation 24°, speed ca. 4 km/h. (b) Highway, antenna S6, elevation 24°, speed ca. 40 km/h.

Figs. 4(a) and 4(b) show the probability density function of the received signal power in a city environment and on a highway. The statistics of the recorded channel are designated as +. The full lines represent the channel model (5) with fitted parameters. The mean received power (0 dB) is related to the power of the unfaded satellite link through (6). The peaking of the density at high values of the received signal power is due to the reception of the direct satellite signal in unshadowed areas.

Figs. 5(a) and 5(b) show the cumulative probability distribution function of the received signal power in a city environment and on a highway. The statistics of the recorded channel are designated as +. The full lines approximating the measurements correspond to the channel model (5). The straight line represents a Rayleigh distribution. From Fig. 5(a) the received signal power is more than 10 dB below the unfaded satellite link with probability 0.60. On a highway, the corresponding probability is 0.085.

Time intervals with a received signal power level below a certain threshold are called fades. Let $p_f(\tau)$ be the probability density that a randomly chosen time instant lies within a fade of duration τ. Fig. 6 shows the probability

$$P_f(T_f) = \int_{T_f}^{\infty} p_f(\tau)\, d\tau \qquad (1)$$

of a time instant being in a fade with duration $\geq T_f$. For example, Fig. 6(a) shows that in a city environment fades below -10 dB relative to the average received signal power and longer than 0.1 s occur for 26% of time. The corresponding number on a highway is 6%, as shown in Fig. 6(b).

Time intervals with the received signal power level about a certain threshold are called connections. Fig. 7 shows the probability $P_c(T_c)$ of a time instant being in a connection of duration $\geq T_c$. Fig. 7(a) shows that in a city environment connections above -10 dB relative to the average received power and longer than 1 s occur for 34% of time. The corresponding number on a highway is 85%, as shown in Fig. 7(b).

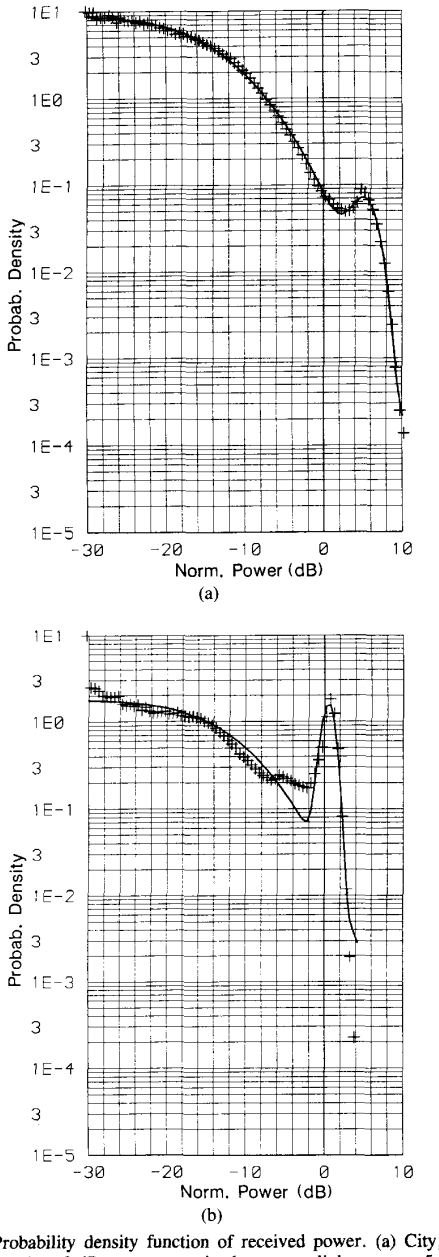

Fig. 4. Probability density function of received power. (a) City, antenna S6, 24° elevation, 0 dB = mean received power = link power -5.2 dB. (b) Highway, antenna S6, 24° elevation, 0 dB = mean received power = link power -0.6 dB.

In the next section, two types of models for the land mobile satellite channel are developed. The analog model attempts to reproduce the stochastic behavior of the received signal in amplitude and in phase. This model can be used for hardware or software simulation of the satellite link for

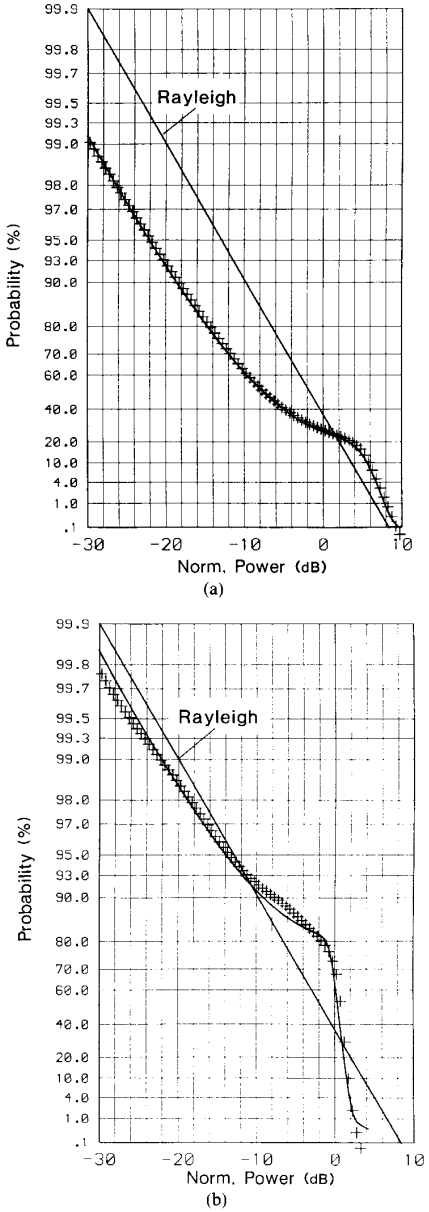

Fig. 5. Complementary cumulative probability distribution function of received power. (a) City, antenna S6, satellite elevation 24°, 0 dB = mean received power = link power − 5.2 dB. (b) Highway, antenna S6, satellite elevation 24°, 0 dB = mean received power = link power − 0.6 dB.

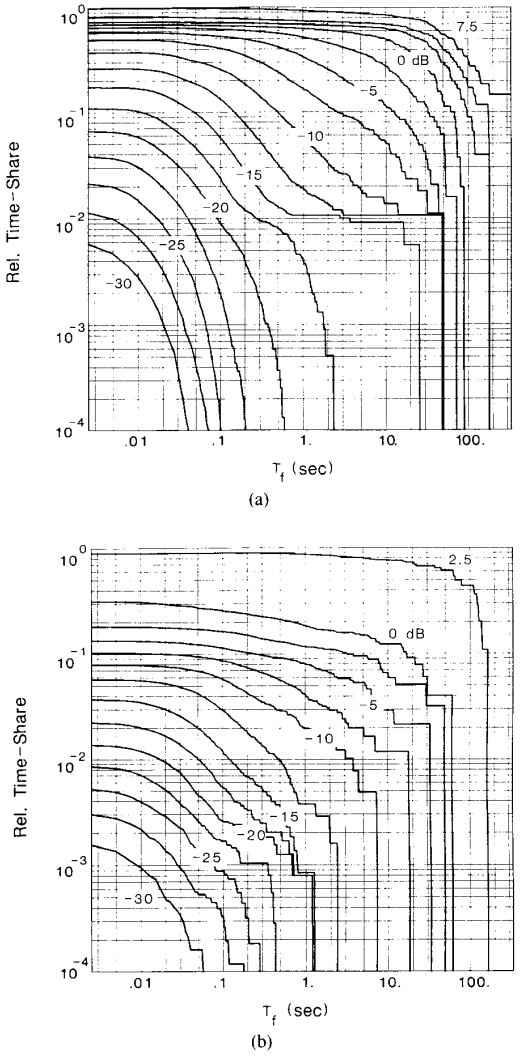

Fig. 6. Time-share of fades with duration $\geqq T_f$. Parameter: threshold relative to mean received power. (a) City, antenna S6, satellite elevation 24°, v = 10 km/h. (b) Highway, antenna S6, satellite elevation 24°, v = 60 km/h.

investigating modulation, coding, and accessing techniques. On the other hand, a digital channel model for reproducing stochastic bit error sequences has the advantage of better mathematical tractability. However, the parameters of the digital channel model depend on the signal-to-noise ratio of the satellite link and on the bit rate.

III. Models of the Land Mobile Satellite Channel

A. Modeling the Probability Density Function of the Received Signal Power

The development of an analog channel model is based on the physical phenomena of multipath fading and shadowing. A first step for this is an analytical approximation of the probability density function of the received signal power [15]. The mobile terminal is assumed as the receiver. However, the channel model is also valid when the mobile terminal is the transmitter.

As indicated by Figs. 2(a) and 2(b), it is useful to distinguish between time intervals with high received signal power ("good" channel state) and time intervals with low power level ("bad" channel state). The good channel state corresponds to areas with unobstructed "view" of the satellite (unshadowed areas), whereas the bad channel state represents areas where the direct satellite signal is shadowed by obstacles. In both of these cases, the satellite signal is reflected from a large number of objects in the surroundings of the mobile receiver. These signal components are received with independently time-varying amplitudes and phases; in the

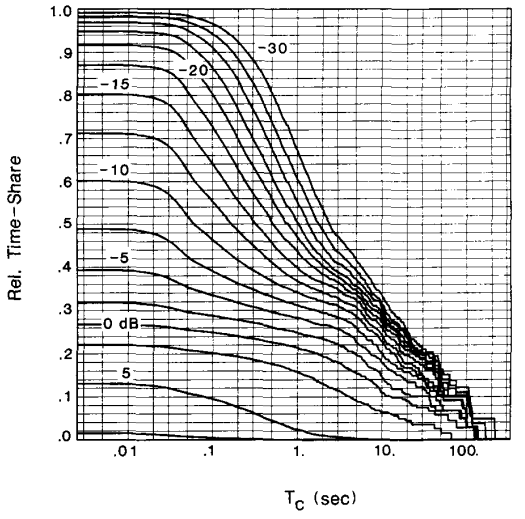

(a)

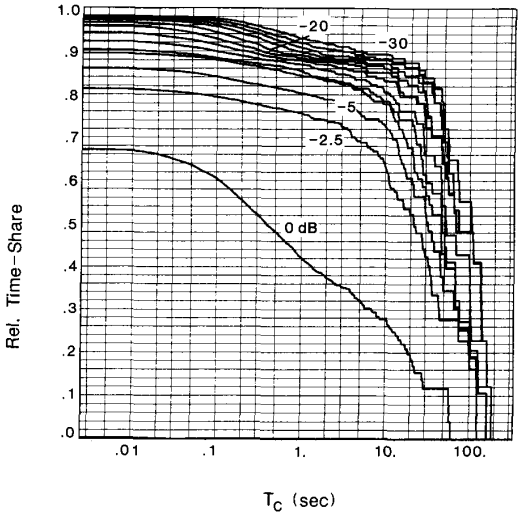

(b)

Fig. 7. Time-share of connections with duration $\geqq T_c$. Parameter: threshold relative to mean received power. (a) City, antenna S6, satellite elevation 24°, v = 10 km/h. (b) Highway, antenna S6, satellite elevation 24°, v = 60 km/h.

limit, these components add up to a complex Raleigh process. When no shadowing is present, this multipath signal is superimposed on the direct satellite signal, with the total received signal amplitude forming a Rician process. The momentary received power S obeys a Rician probability density:

$$p_{\text{Rice}}(S) = ce^{-c(S+1)}I_0(2c\sqrt{S}). \tag{2}$$

Here c is the direct-to-multipath signal power ratio (Rice-factor) and I_0 is the modified Bessel function of order zero. The power of the unfaded satellite link is normalized to unity. Under the condition of no shadowing the mean received total power is $\mathrm{E}\{S \mid \text{no shadowing}\} = 1 + 1/c$.

When shadowing is present, it is assumed that no direct signal path exists and that the multipath fading has a Rayleigh characteristic with short-term mean received power S_0. The probability density function of the received power conditioned on mean power S_0 is

$$p_{\text{Rayl.}}(S \mid S_0) = \frac{1}{S_0}\exp(-S/S_0). \tag{3}$$

The slow shadowing process results in a time varying short-term mean received power S_0 for which a lognormal distribution is assumed:

$$p_{\text{LN}}(S_0) = \frac{10}{\sqrt{2\pi}\,\sigma \ln 10}\cdot\frac{1}{S_0}\exp\left[-\frac{(10\log S_0 - \mu)^2}{2\sigma^2}\right]. \tag{4}$$

Here μ is the mean power level decrease (in decibels) and σ^2 is the variance of the power level due to shadowing. With (3) and (4), the received power is described by a Rayleigh/lognormal distribution which is often used for the terrestrial land mobile channel [16].

In order to get the resulting probability density function of the received signal power, the densities (2)-(4) must be properly combined. To this end the time-share of shadowing, A is defined, and the resulting probability density function becomes

$$p(S) = (1 - A)\cdot p_{\text{Rice}}(S) + A \cdot \int_0^\infty p_{\text{Rayl.}}(S \mid S_0)\, p_{\text{LN}}(S_0)\, dS_0 \tag{5}$$

where the integral expression results from the theorem of total probability. $p(S)$ is independent of vehicle velocity v which is assumed constant. In [17], a different approach suitable to foliage attenuation is described, assuming a lognormally distributed direct signal plus a Rayleigh distributed multipath signal with constant power.

The 0 dB value in Figs. 2 and 4-7 corresponds to the mean received power (the power of the unfaded link normalized to unity):

$$\mathrm{E}\{S\} = (1 - A)\cdot\left(1 + \frac{1}{c}\right) + A \cdot 10^{\ln 10\cdot(\sigma/10)^2/2 + \mu/10}. \tag{6}$$

For different satellite elevations, different types of environments, and different antennas, the parameters A, c, μ, and σ as given in Table II have been determined from the statistics of the recordings by a least square curve-fitting procedure. Table II is limited to city and highway environments which represent the worst and best case within the range of environments.

Using parameter values given in Table II, the probability

TABLE II
PARAMETERS OF THE ANALOG AND DIGITAL CHANNEL MODEL.[1] THE NUMERICAL VALUES OF ϵ_g AND ϵ_b REFER TO DPSK MODULATION WITH $E_{\text{link}}/N_0 = 10$ dB

Satellite Elevation	Environment	Antenna	A	10 log c	μ	σ	D_g	D_b	ϵ_g	ϵ_b
13°	Highway	C3	0.24	10.2 dB	−8.9 dB	5.1 dB	90 m	29 m	$1.6 \cdot 10^{-3}$	0.23
	City	C3	0.89	3.9 dB	−11.5 dB	2.0 dB	9 m	70 m	$1.4 \cdot 10^{-2}$	0.29
18°	City	C3	0.80	6.4 dB	−11.8 dB	4.0 dB	8 m	32 m	$7.2 \cdot 10^{-3}$	0.29
	City	D5	0.80	5.5 dB	−10.0 dB	3.7 dB	8 m	33 m	$9.5 \cdot 10^{-3}$	0.25
21°	New City	D5	0.57	10.6 dB	−12.3 dB	5.0 dB	45 m	60 m	$1.3 \cdot 10^{-3}$	0.30
	Highway	D5	0.03	16.6 dB	−7.1 dB	5.5 dB	524 m	15 m	$1.1 \cdot 10^{-4}$	0.19
	Highway	S6	0.03	18.1 dB	−7.9 dB	4.8 dB	514 m	17 m	$7.6 \cdot 10^{-5}$	0.20
24°	Old City	C3	0.66	6.0 dB	−10.8 dB	2.8 dB	27 m	52 m	$8.3 \cdot 10^{-3}$	0.27
	Old City	D5	0.78	9.3 dB	−12.2 dB	4.4 dB	21 m	76 m	$2.3 \cdot 10^{-3}$	0.30
	Old City	S6	0.79	11.9 dB	−12.9 dB	5.0 dB	24 m	88 m	$7.0 \cdot 10^{-4}$	0.32
	Highway	C3	0.25	11.9 dB	−7.7 dB	6.0 dB	188 m	62 m	$6.8 \cdot 10^{-4}$	0.20
	Highway	S6	0.19	17.4 dB	−8.1 dB	4.2 dB	700 m	160 m	$9.0 \cdot 10^{-5}$	0.21
34°	City	C3	0.58	6.0 dB	−10.6 dB	2.6 dB	24 m	33 m	$8.3 \cdot 10^{-3}$	0.27
	City	M2	0.72	10.0 dB	−11.9 dB	4.9 dB	21 m	55 m	$1.7 \cdot 10^{-3}$	0.29
	City	S6	0.60	9.5 dB	−12.2 dB	2.0 dB	20 m	31 m	$2.1 \cdot 10^{-3}$	0.31
	Highway	C3	0.008	11.7 dB	−8.8 dB	3.8 dB	1500 m	12 m	$7.6 \cdot 10^{-4}$	0.22
	Highway	S6	0.007	16.7 dB	−13.4 dB	5.3 dB	1500 m	11 m	$1.1 \cdot 10^{-4}$	0.32
43°	City	C3	0.54	5.5 dB	−13.6 dB	3.8 dB	42 m	49 m	$9.5 \cdot 10^{-3}$	0.34
	City	M2	0.65	11.0 dB	−15.4 dB	5.4 dB	16 m	29 m	$1.1 \cdot 10^{-3}$	0.36
	City	S6	0.56	6.5 dB	−15.6 dB	3.8 dB	51 m	65 m	$7.0 \cdot 10^{-3}$	0.38
	Highway	C3	0.002	14.8 dB	−12.0 dB	2.9 dB	8300 m	17 m	$2.0 \cdot 10^{-4}$	0.30
	Highway	M2	0.002	17.3 dB	−13.8 dB	2.0 dB	8300 m	17 m	$9.2 \cdot 10^{-4}$	0.35

[1]With respect to results listed in [15], this table contains some differences which are due to improved techniques of statistical evaluation.

density according to (5) and the corresponding distribution function are included in Figs. 4 and 5 as full lines. The fits show good agreement with the statistics of the recorded signal power. In Fig. 4 the Rician density which forms a pronounced peak at the power level of the unfaded satellite link can clearly be distinguished from the Rayleigh/log-normal density which increases for low power level. The distribution functions shown in Fig. 5 exhibit a bend at -1 dB for highway and at 4 dB for city, respectively. Above these levels the Rician fading (unshadowed areas) is predominant, characterized by the straight part of the line. At levels below the bend lognormal shadowing is present.

It may be expected that a transmission during shadowed intervals will not be successful with a realistic link budget. Therefore, the most important parameter of the land mobile satellite channel is the time-share of shadowing, A. 1-A is the time-share during which a transmission is possible and therefore represents a rough estimate for the achievable gross throughput of digital transmission systems. Fig. 8 shows the parameter 1-A for different satellite elevations. The symbols represent single recording experiments. The lines show that the time-share of unshadowed intervals, 1-A tends to increase with elevation (shadowing decreases). The values of 1-A indicate that on highways substantial data throughput can be achieved for all elevations tested, whereas in cities the throughput is rather small for low elevation.

During the periods without shadowing, the channel is modeled as a Rician channel (2), with the fading behavior described by Rice-factor c. Large values of c indicate few multipath fading ($c \to \infty$ for the Gaussian channel) resulting in good transmission characteristics. Small values of c correspond to severe fading ($c = 0$ for the Rayleigh channel).

B. Bit Error Rate for Continuous Transmission

The error probability of a received symbol is determined by the ratio of symbol energy E_s and one-sided noise power spectral density N_0. The received symbol energy E_s depends on the signal-to-noise ratio E_{link}/N_0 of the unfaded link and on the amount of shadowing and fading within the symbol duration. For reasonably high bit rates and realistic mobile speed v the fading varies slowly compared to the bit rate [18], then, the received signal power may be considered constant during one symbol interval. For a DPSK symbol received with momentary power S normalized to the power of the unfaded satellite link the error probability is

$$\text{BER}(S) = \frac{1}{2} \exp\left(-SE_{\text{link}}/N_0\right). \tag{7}$$

With the probability density function $p(S)$ of the received power the mean BER becomes

$$\text{BER} = \int_0^\infty \text{BER}(S)\, p(S)\, dS. \tag{8}$$

The mean BER may be evaluated by numerical integration of (8), [15]. Based on (5), analytic expressions for the mean BER of DPSK and noncoherent FSK transmission are derived in [19].

Fig. 9 shows the resulting mean BER for DPSK transmission. The curves show that in shadowed areas, a prohibitively high link power would be necessary to reduce the BER to an acceptable range. In unshadowed areas a BER of 10^{-4} is achievable with moderate link power in spite of the presence of multipath fading. Using forward error correction (FEC) coding and interleaving, the link behavior may be improved

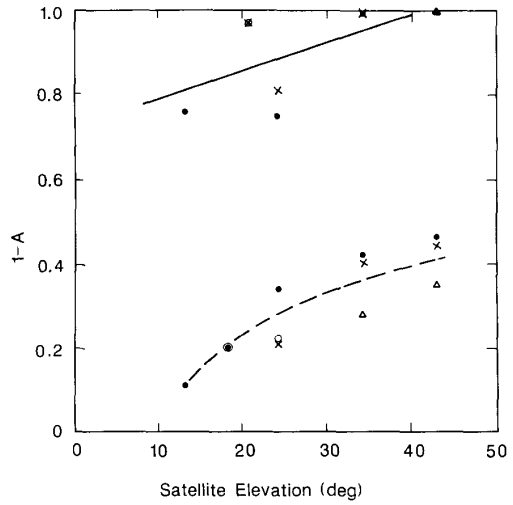

Fig. 8. Time-share of unshadowed time intervals versus satellite elevation. Lines represent all antennas.
- ● antenna C3
- △ antenna M2
- ○ antenna D5
- × antenna S6
- —— highway
- --- city.

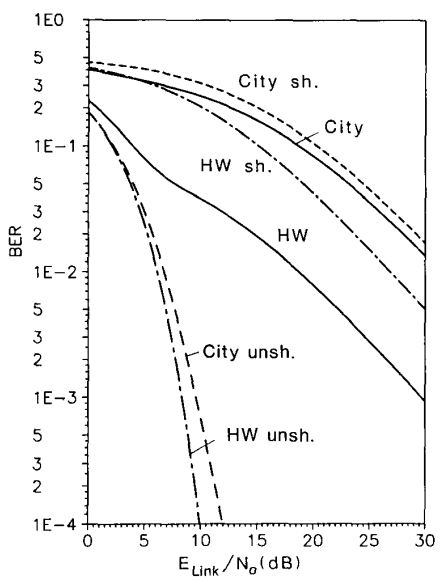

Fig. 9. Mean BER for DPSK transmission. Lines are showing BER for shadowed (sh.) and unshadowed (unsh.) areas in cities and on highways (HW). Full lines show combined BER. Antenna S6, 24° satellite elevation.

further [20]. The full lines in Fig. 9 show the BER averaged over both, shadowed and unshadowed areas.

C. Analog Model of the Land Mobile Satellite Channel

Fig. 10 shows a dynamic model of the land mobile satellite channel that reproduces the probability density function of the received signal power as well as the dynamic behavior of the fading and shadowing process. The transmitted signal $s(t)$ is deteriorated by multiplicative fading $a(t)$ and additive white Gaussian noise $n(t)$ with power spectral density N_0. The resulting received signal is

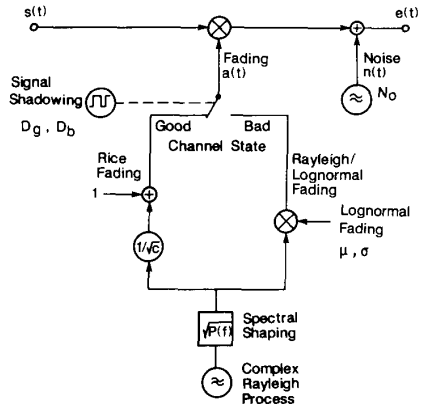

Fig. 10. Dynamic model of the land mobile satellite channel. The signals $s(t)$, $n(t)$, $e(t)$, and the fading process $a(t)$ are complex valued.

$$e(t) = s(t) \cdot a(t) + n(t). \tag{9}$$

It should be noted that the fading process $a(t)$ produced by the channel model is complex valued. The concept of multiplicative fading can be applied when the bandwidth of the transmitted signal is small compared to the coherence bandwidth of the fading. Measurements in urban environments [21] have shown that the coherence bandwidth of the land mobile channel is usually in the order of 100 kHz or larger. Therefore, the channel model according to Fig. 10 may be used for signal bandwidths up to several tens of kilohertz. Cochannel interference and adjacent channel interference are not considered in this paper, but may be easily included in the model if required.

According to Fig. 2 and Section III-A, the fading process $a(t)$ is "switched" between Rician fading, representing unshadowed areas with high received signal power (good channel state) and Rayleigh/lognormal fading, representing shadowed areas with low received signal power (bad channel state). This is a reasonable approximation to reality resulting in a simplified channel model. The characteristics of the switching process between shadowed and unshadowed sections can be approximated by a Markov model [22]. For a given speed v m/s and bit rate R b/s, the transition probabilities p_{gb} and p_{bg} can be related to the bit duration. According to the Markov model, the mean duration of a period of good (bad) channel state is given by

$$D_g \text{ bits} = \frac{1}{p_{gb}} = \frac{R}{v} D_g \text{ m}$$

$$D_b \text{ bits} = \frac{1}{p_{bg}} = \frac{R}{v} D_b \text{ m}. \tag{10}$$

The probability that a good (bad) channel state lasts longer than n bits is

$$p_g(> n) = p_{gg}^n$$

$$p_b(> n) = p_{bb}^n. \tag{11}$$

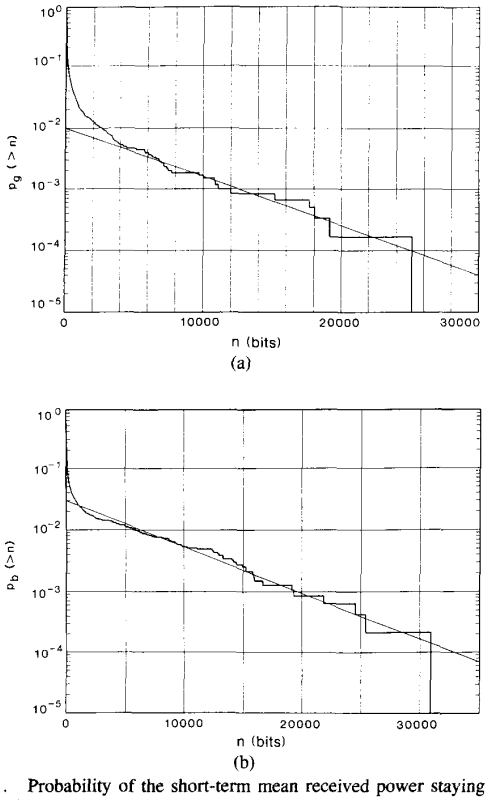

Fig. 11. Probability of the short-term mean received power staying above (a) or below (b) a threshold for more than n bit durations. The threshold corresponds to the time-share of shadowing, A. The probabilities are normalized such that $p_g(>0) = 1 - A$ and $p_b\ (>0) = A$. City environment, satellite elevation 21°, v = 40 km/h, R = 1200 b/s.

Plotting these probabilities in a semilogarithmic scale results in straight lines with slopes log p_{gg} and log p_{bb}, respectively.

To verify if the shadowing process of the recorded channels can be approximated by a Markov model, the probability of the short-term mean received signal power staying above (below) a threshold for longer than n bit durations has been evaluated. Periods of the received signal power above and below the threshold are considered good and bad channel states, respectively. The threshold must be determined such that the time-share when the received signal power is below the threshold is equal to A. The time-share A of shadowing is known from curve fitting, Table II. The threshold can be determined from the probability distribution function of the received signal power. Fig. 11(a) and (b) shows probabilities of good (bad) channel states lasting longer than n bit in duration as evaluated from the recorded channel. The straight lines represent the approximation according to (11).

For short duration, the statistics of the recorded channel deviated from the straight lines. This is caused by level crossings due to fading. For longer duration, however, the Markov process is a good approximation. The transition probabilities of the Markov model can be derived from the probability distributions $p_g(>n)$ and $p_b(>n)$ of the recording by approximating them with straight lines, as shown in Figs. 11(a) and 11(b). The mean duration of a good (bad) channel state follows from (10), and

$$p_{gb} = 1 - p_{gg}$$
$$p_{bg} = 1 - p_{bb}. \tag{12}$$

The time-share of shadowing, A, is related to the durations D_g and D_b by

$$A = \frac{D_b}{D_g + D_b}. \tag{13}$$

The duration D_g and D_b evaluated from the distributions $p_g(>n)$ and $p_b(>n)$ usually do not satisfy (13) exactly. Therefore, mean values are computed according to

$$\overline{D_g} = \frac{1}{2}\left[D_g + \frac{1-A}{A}D_b\right]$$
$$\overline{D_b} = \frac{1}{2}\left[\frac{A}{1-A}D_g + D_b\right]. \tag{14}$$

For the measurements listed in Table II, the durations D_g m and D_b m were determined by (14).

Having described the dynamic behavior of the shadowing process, the fading process is considered below. As explained in Section III-A and indicated by Fig. 10, the received multipath signal may be modeled as a Rayleigh process having Rayleigh distributed amplitude and uniformly distributed phase. This process may be generated by complex addition of two independent stationary Gaussian processes. The spectral properties of the complex Rayleigh process are defined by an appropriate filter. In order to model the fading in city environments, a filter may be chosen that approximates [18, eq. (20)]. For rural environment, the filter should have a slowly decreasing low-pass characteristic as shown in Fig. 3(b). As a compromise, a flat low-pass filter with a bandwidth of maximum Doppler frequency may be used for all types of environments.

Based on the filtered Rayleigh process, the Rician fading is produced by attenuating the Rayleigh process to power of $1/c$ and adding a value of unity to represent the direct satellite signal component. The Rayleigh/lognormal fading is generated by multiplying the Rayleigh process with a slow lognormal shadowing process. This approach has the advantage that very deep fades can be reproduced which is not possible when assuming constant multipath power. Situations with partly shadowed line-of-sight signal are also included in the Rayleigh/log-normal fading. In order to approximate the dynamic behavior of the log-normal shadowing, the short-term mean received signal power S_0 may be chosen according to its probability density (4) independently for each shadowing interval and kept constant during that interval.

D. Digital Model of the Land Mobile Satellite Channel

Digital channel models describe the bit error process on the physical link and therefore give a higher level of abstraction. Due to the dominance of the shadowing process, the two-state Gilbert-Elliott model [23] appears very suitable for the land mobile satellite channel. The dynamics of the state

transitions are very similar to those described above for the transitions between the good and bad states in the analog model. Measurements and simulations have shown that the underlying Markov-chain can be described by the same probabilities p_{gb} and p_{bg} from (12) or by a state diagram in [24].

Once p_{gb} and p_{bg} are given, the bit error rate values ϵ_g and ϵ_b in the good and bad states, respectively, can be obtained [19]. The results are given in Table II for a DPSK signal with $E_{\text{link}}/N_0 = 10$ dB. The values of ϵ_g and ϵ_b may also be obtained from the stored channel measurements.

IV. Block Error Statistics and Model Comparison

In packet data communications, the blocks of data can be protected against transmission errors either by forward error correction (FEC) or by automatic repeat request (ARQ). For a plain ARQ scheme with error detection, the probability of a data block containing no errors is directly related to the throughput of the ARQ scheme. If a t-error correcting block code is applied, the probability of correct block decoding equals the probability of at most t errors occurring in the data block. Investigations concerning the achievable throughput of ARQ schemes as well as the optimization of code rate, signaling rate, and data block length are contained in [15] and [25]. No bit interleaving is assumed here because the bit error rate in the good state is reasonably low and in the bad state is very high. Without interleaving, it is possible to have a complete data block in an interval of good channel state. Thus an ARQ scheme exploits time intervals with good link characteristics for reliable data transmission.

Transmission channels with memory such as the land mobile satellite channel which has a strong statistical dependency among error gaps can be characterized by multigap distribution or by error correlation function [24], [26]. With error gap ν being the number of consecutive correctly received symbols between errors plus 1, the gap density $f_A(\nu)$ is defined as

$$f_A(\nu) = P(e_1 = 0 \cap e_2 = 0 \cap \cdots \cap e_{\nu-1} = 0 \cap e_\nu = 1 \mid e_0 = 1) \quad (15)$$

where e_i is 0 for an error-free symbol and 1 for an error.

The complementary gap distribution function $F_A(\nu)$ which is the probability of an error gap being larger than ν, is given by

$$F_A(\nu) = 1 - \sum_{j=1}^{\nu} f_A(j). \quad (16)$$

The gap density $f_A(j)$ is related to the block error density $P(m, n)$ by [26]

$$f_A(j) = \frac{1}{p}\left[P(0, j-1) - 2P(0, j) + P(0, j+1)\right], \quad (17)$$

where p is the mean bit error probability.

Inserting (17) into (16) and assuming that $P(0, 0) = 1$ and $P(0, 1) = 1 - p$, the complementary gap distribution function becomes

$$F_A(\nu) = \frac{P(0, \nu) - P(0, \nu + 1)}{p}. \quad (18)$$

The behavior of the recorded channel and its comparison with the channel models in terms of block error density $P(m, n)$, complementary gap distribution $F_A(\nu)$, and conditional block error probability $P_{F|F}$ will be given where $P_{F|F}$ is the probability that a block contains errors after decoding under the condition that the preceding block also contained errors. These criteria are well related to the transmission of data packets and are easy to measure in a real system. The error correlation function was not used because the calculation requirement was extensive, and the results did not show clearly the channel behavior in various environments.

For the digital model, the block error probability density $P(m, n)$ can be analytically derived from the state transition probabilities. With Z being the state "good" or "bad" and P_Z the state probability, $P(m, n)$ becomes

$$P(m, n) = \sum_{(Z)} P(m, n \mid Z) P_Z. \quad (19)$$

The conditional probabilities $P(m, n \mid Z)$ are calculated using recursion, starting with the first bit of a block. This result is found in [22] and [23] and is not repeated here. The block error probability density for the recorded measurements is directly determined by a window of blocklength n sliding along the measurement sequence and calculating the probability of m errors within the window. The average of all window results gives a very good approximation of the probability $P(m, n)$ as the number of samples is very large.

For two typical environments, city and highway, $P(m, n)$ is depicted in Fig. 12. Each diagram compares the results of the stored measurements, the analog model and the digital model for a block length of $n = 100$ bits. For small error numbers m, the models match the measurement curves very well. This region is of most interest because these few errors could be corrected by an error correcting code. The Gilbert–Elliott model exhibits a deep floor for the probability of 2–15 errors. The steep slope of the curve above its maximum stems from the fact that error events within the bad state are generated independently and that corresponds to the binomial distribution function. A comparison of the full line (recording) and the dashed line (simulation using the analog channel model) shows rather good agreement. This shows that the channel model, Fig. 10, not only reproduces the probability density function of the received signal power but models the dynamic behavior of the bit error sequence as well.

The information of the complementary gap distribution $F_A(\nu)$ is completely contained in the block error probability densities $P(m, n)$, $n = \nu$, $\nu + 1$ as indicated by (18). Fig. 13 shows $F_A(\nu)$ for the same recordings and channel models as Fig. 12. Here, the bad channel state corresponds to small values of ν, and the good channel state corresponds to large ν.

The performance of forward error correction is determined by the block error probability, P_F, that is, a block contains

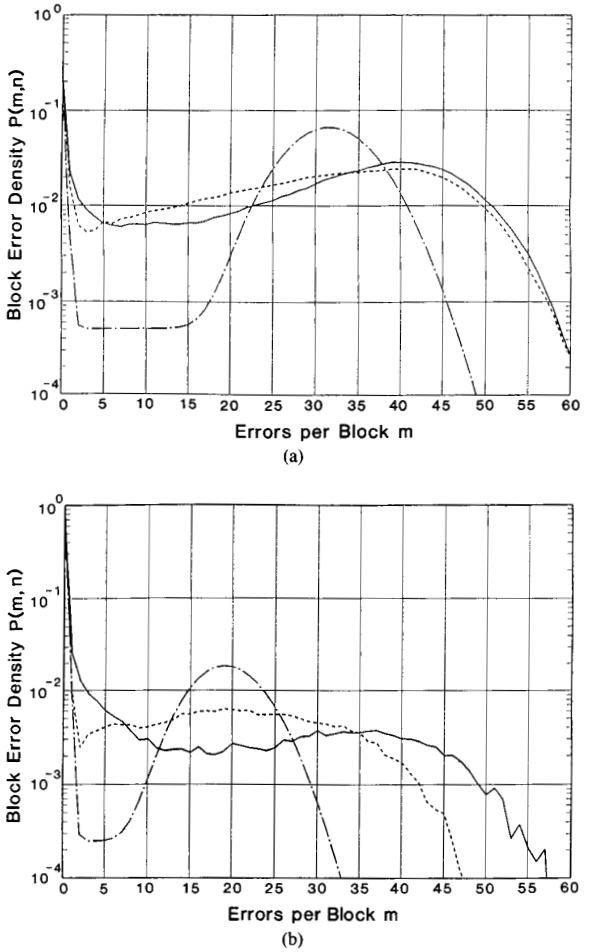

Fig. 12. Block error density $P(m, n)$. Satellite elevation 24°, blocklength n = 100 bits, E_{link}/N_0 = 10 dB, R = 1200 b/s. (a) City, antenna S6, v = 40 km/h. (b) Highway, antenna S6, v = 90 km/h.
—— channel recordings
---- analog channel model
-·-·-· Gilbert–Elliott model.

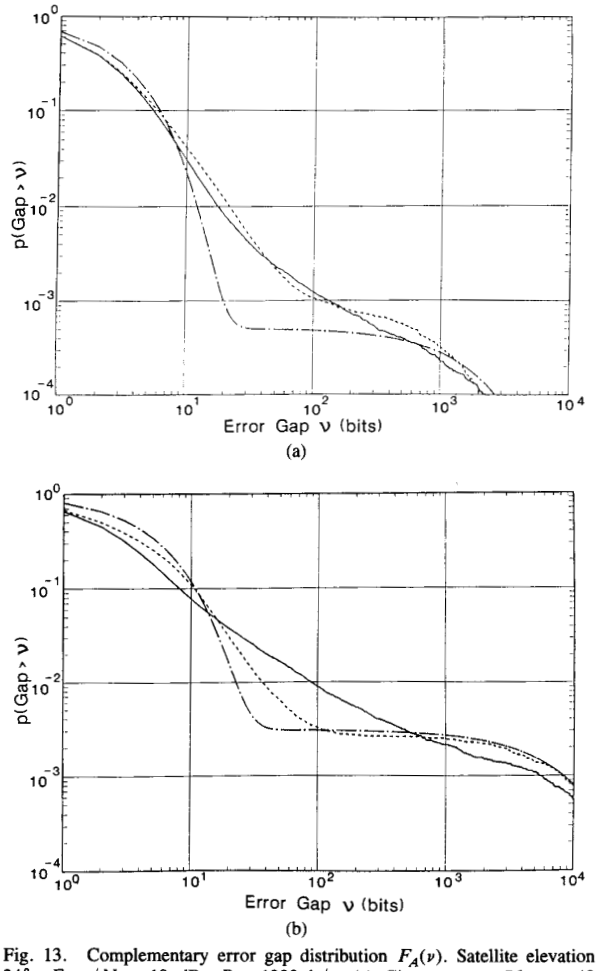

Fig. 13. Complementary error gap distribution $F_A(\nu)$. Satellite elevation 24°, E_{link}/N_0 = 10 dB, R = 1200 b/s. (a) City, antenna S6, v = 40 km/h. (b) Highway, antenna S6, v = 90 km/h.
—— channel recordings
---- analog channel model
-·-·-· Gilbert–Elliott model.

more errors than the code can correct. With bounded distance decoding, a block code can correct up to t errors in a block of length n and the block error probability, P_F can be calculated from

$$P_F = \sum_{m=t+1}^{n} P(m, n). \tag{20}$$

Due to very strong channel memory, a mean state duration is in the order of thousands of bits, and it is obvious that packet errors in succeeding blocks are highly dependent. This must be considered for the design of ARQ schemes. The dependence of block errors is shown by means of the conditional block error probability, $P_{F|F}$. For the Gilbert–Elliott model, $P_{F|F}$ can be analytically derived [22].

The curves of $P_{F|F}$ are shown in Fig. 14. The abscissa shows the distance between two defective blocks in bits. The conditional error curves, $P_{F|F}$ approach asymptotically the unconditioned block error probability, P_F which is 0.78 for city environment and 0.18 for highway. But, this happens only after the transmission of several thousands of bits. Long correlation is seen in the highway environment where $P_{F|F}$ is still greater than P_F after ten-thousand bits or an 8.3-s delay. In all cases, the models approximate reality quite well.

V. Conclusion

The land mobile satellite channel has been recorded and subjected to a statistical evaluation. An analog channel model was developed that can readily be used for fading simulation purposes. This channel model is largely characterized by the time-share of shadowing, A, and the Rice-factor, c, describing the channel during unshadowed periods. Alternatively, the land mobile satellite channel can be represented by a two-state Gilbert–Elliott model. A comparison of block error

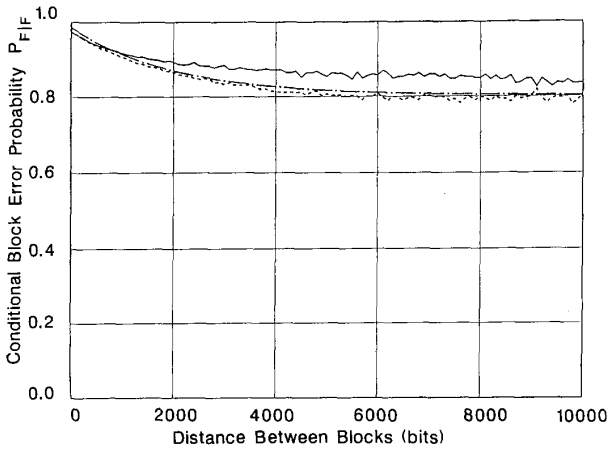

(a)

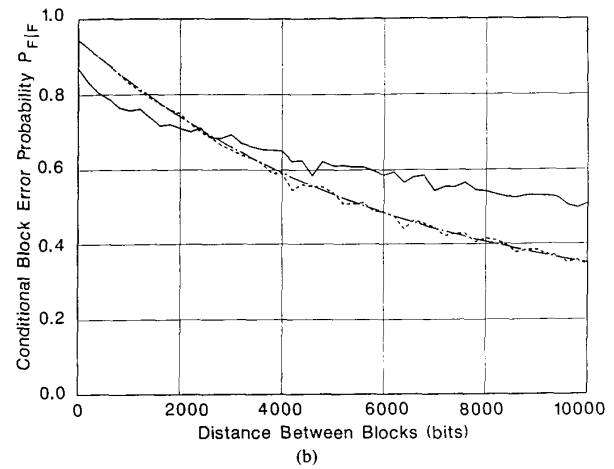

(b)

Fig. 14. Conditional block error probability $P_{F|F}$ versus block distance. Satellite elevation 24°, blocklength n = 100 b, t = 0, E_{link}/N_0 = 10 dB, R = 1200 b/s. (a) City, antenna S6, v = 40 km/h. (b) Highway, antenna S6, v = 90 km/h.
—— channel recordings
---- analog channel model
-·-·-· Gilbert-Elliott model.

statistics shows good agreement between the recorded channel and the models. In combination with their parameter values, the developed channel models represent useful tools for the design and analysis of data transmission schemes. Moreover, the models show that reliable and efficient data transmission via the land mobile satellite channel should be achievable, if the transmission scheme is suitably adapted to the channel behavior.

Acknowledgment

The permission by ESA and INMARSAT to use the MARECS test carrier is acknowledged. The provision of antennas by the DLR institute of RF-techniques is appreciated. Furthermore, the authors would like to thank Prof. J. Hagenauer for valuable discussions and support.

References

[1] F. Naderi, "An advanced generation land mobile satellite system and its critical technologies, " in *Proc. Nat. Telesystems Conf.*, TX, Nov. 1982.
[2] R. R. Lovell, G. H. Knouse, and W. J. Weber, "An experiment to enable commercial mobile satellite service," in *Proc. Nat. Telesystems Conf.*, TX, Nov. 1982.
[3] P. M. Bourdeau, R. W. Breithaupt, and J. L. McNally, "The Canadian mobile satellite program," in *Proc. Nat. Telesystems Conf.*, TX, Nov. 1982.
[4] S. Miura, "Experimental mobile satellite system for communications using Engineering Test Satellite-V (ETS-V/EMSS-C)," presented at the IAF '84, Lausanne, Switzerland, Oct. 1984.
[5] M. Wagg, "MOBILESAT, Australia's own," in *Proc. Int. Mobile Sat. Conf.*, Ottawa, Canada, June 1990.
[6] R. Rogard, "A land-mobile satellite system for digital communications in Europe," in *Proc. ESA Workshop*, Noordwijk, the Netherlands, June 1986.
[7] G. Berzins, "Communications on the move-INMARSAT's services in the future" in *Proc. Fourth Int. Conf. on Satellite Systems for Mobile Commun. and Navigation*, London, U.K., Oct. 1988.
[8] I. E. Casewell, I. C. Ferebee, and M. Tomlinsons, "A satellite paging system for land mobile users," in *Proc. Fourth Int. Conf. on Satellite Systems for Mobile Commun. and Navigation*, London, U.K., Oct. 1988.
[9] J. Hagenauer and E. Lutz, "Forward error correction coding for fading compensation in mobile satellite channels," *IEEE J. Select. Areas Commun.*, vol. SAC-5, pp. 215-225, Feb. 1987.
[10] G. C. Hess, "Land-mobile satellite excess path loss measurements," *IEEE Trans. Veh. Technol.*, vol. VT-29, pp. 290-297, May 1980.
[11] C. Loo, "Measurements and models of a land mobile satellite channel and their applications to MSK signals," *IEEE Trans. Veh. Technol.*, vol. VT-35, pp. 114-121, Aug. 1987.
[12] J. S. Butterworth, "Propagation measurements for land mobile satellite systems at 1542 MHz," CRC Tech. Note 723, Ottawa, Canada, Aug. 1984.
[13] W. C. Y. Lee, *Mobile Communications Design Fundamentals*. Indianapolis, IN: Howard W. Sams, 1986.
[14] J. Hagenauer and W. Papke, "Data transmission for maritime and land mobiles using stored channel simulation," in *Proc. IEEE 32nd Veh. Technol. Conf. 1982*, San Diego, CA, pp. 379-383.
[15] E. Lutz, W. Papke, and E. Plöchinger, "Land mobile satellite communications—channel model, modulation and error control," in *Proc. 7th Int. Conf. on Digital Satellite Commun. 1986*, Munich, Germany, pp. 537-543.
[16] F. Hansen and F. Meno, "Mobile fading—Rayleigh and lognormal superimposed," *IEEE Trans. Veh. Technol.*, vol. VT-26, pp. 332-335, Nov. 1977.
[17] C. Loo, "A statistical model for a land mobile satellite link," *IEEE Trans. Veh. Technol.*, vol. VT-34, pp. 122-127, Aug. 1985.
[18] R. H. Clarke, "A statistical theory of mobile radio reception," *Bell Syst. Tech. J.*, vol. 47, pp. 957-1000, July/Aug. 1968.
[19] D. Cygan, "Analytical evaluation of average bit error rate for the land mobile satellite channel," *Int. J. Satell. Commun.*, vol. 7, pp. 99-102, Apr. 1989.
[20] E. Lutz, "Code and interleaver design for data transmission over fading channels," in *Proc. GLOBECOM '84*, Atlanta, GA, pp. 381-386.
[21] D. C. Cox and R. P. Leck "Correlation bandwidth and delay spread multipath propagation statistics for 910 MHz urban mobile radio channels," *IEEE Trans. Commun.*, vol. COM-23, pp. 1271-1280, Nov. 1975.
[22] D. Cygan, M. Dippold, and J. Finkenzeller, "Models for the land mobile satellite channel," *Archiv. Elec. Übertr.*, vol. 42, pp. 329-339, Nov./Dec. 1988.
[23] E. O. Elliott, "Estimates of error rates for codes on burst-noise channels," *Bell Syst. Tech. J.*, vol. 42, pp. 1977-1997, Sept. 1963.
[24] L. N. Kanal and A. R. K. Sastry, "Models for channels with memory and their applications to error control," *Proc. IEEE*, vol. 66, pp. 724-744, July 1978.
[25] E. Lutz, "Simulation of FEC/ARQ data transmission using stored land mobile satellite channels," in *Proc. IEEE 36th Veh. Technol. Conf. 1986*, Dallas, TX, pp. 109-115.
[26] J.-P.A. Adoul, "Error intervals and cluster density in channel modeling," *IEEE Trans. Inform. Theory*, vol. IT-20, pp. 125-129, Jan. 1974.

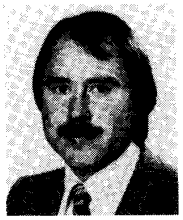

Erich Lutz received the Ing. grad. degree from the Fachhochschule Augsburg in 1972, the Dipl.-Ing. degree from the Technische Universität München in 1977, and the Dr.-Ing. degree from Military University Munich, in 1983.

During 1977 to 1982 he worked in the area of digital transmission over cables and optical fibers at the Technical University and the Military University Munich. Since 1982 he has been with the Institute for Communication Technology of the German Aerospace Research Establishment (DLR) in Oberpfaffenhofen, Germany. Since 1986 he has been head of the Digital Network section of the institute. His research interests include digital transmission techniques, channel coding applications, ARQ techniques and protocols, in particular for mobile communication channels.

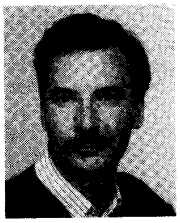

Daniel Cygan was born in Berlin, Germany, on April 2, 1957. He received the Dipl.-Ing. degree in electrical engineering from the Technische Universität München, Munich, Germany, in 1986.

Since 1986 he has been with the Institute of Communications Technology, German Aerospace Research (DLR), Oberpfaffenhofen, Germany. His areas of current interest include coding theory and adaptive ARQ strategies, in particular for mobile communications.

Michael Dippold received the Dipl.-Ing. and the Dr.-Ing. degrees in electrical engineering in 1985, both from the Technische Universität München, Munich, Germany, in 1978 and 1985, respectively.

He worked as a scientific assistant for the Technical University in Munich until 1985. In 1985/1986 he was with Bell Northern Research, Canada, working on high-speed optical transmission and coherent optical systems. From 1986-1991 he was with the Institut for Communications of the German Aerospace Research (DLR) at Oberpfaffenhofen. He worked on packet transmission and multiple access problems particularly in packet radio and satellite systems. Since April 1991 he has been a Professor at the University in Munich, Germany.

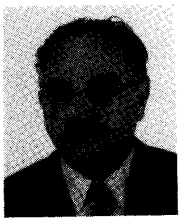

Frank Dolainsky received the Dipl.-Ing. degree from the Technische Hochschule Wien, Vienna, Austria, in 1960.

Since 1968 he has been with the Institute for Communication Technology of the German Aerospace Research Establishment (DLR), Oberpfaffenhofen, Germany.

Wolfgang Papke received the Dipl.-Ing. (FH) degree from the Fachhochschule Konstanz in 1966.

Since 1966 he has been with the Theory Group of the German Aerospace Research Establishment (DLR), Oberpfaffenhofen, Germany. Since 1976 he has been involved in several research projects for mobile communications. He is responsible for the hardware and operational aspects of field tests and lab simulations.